Journal of

Applied and Computational Mechanics

Shahid Chamran
University of Ahvaz

Stagnation Flow of Eyring-Powell Hybrid Cu-Al₂O₃/Water Nanofluid Towards a Riga Plate with Newtonian Heating

Ahlam Aljabali[1], Abdul Rahman Mohd Kasim[1,2], Najiyah Safwa Khashi'ie[3], Iskandar Waini[3],
Noor Amalina Nisa Ariffin[4]

[1] Centre for Mathematical Sciences, University Malaysia Pahang, Lebuhraya Tun Razak, Pahang, Gambang 26300, Pahang, Malaysia, Email: rahmanmohd@ump.edu.my

[2] Centre for Research in Advanced Fluid and Process, University Malaysia Pahang, Lebuhraya Tun Razak, Pahang, Gambang, 26300, Malaysia, Email: rahmanmohd@ump.edu.my

[3] Fakulti Teknologi dan Kejuruteraan Mekanikal, Universiti Teknikal Malaysia Melaka, Hang Tuah Jaya, Durian Tunggal 76100, Melaka, Malaysia, Email: najiyah@utem.edu.my (N.S.K); iskandarwaini@utem.edu.my (I.W.)

[4] Faculty of Computer & Mathematical Sciences, Universiti Teknologi MARA (UiTM) Pahang Branch, Jengka Campus, 26400 Bandar Tun Abdul Razak Jengka, Pahang, Malaysia, Email: amalinanisa@uitm.edu.my

Abstract. The problem of convective heat transfers of Eyring-Powell conveying Copper (Cu) coupled with alumina (Al₂O₃) are employed as the combination of particles, along with water as the base fluid over a vertical Riga plate is numerically addressed. The performance of heat transmission is influenced by the electromagnetohydrodynamic (EMHD) imposed produced from the Riga plate, and it could be used to postpone boundary layer separation. A model in the form of Partial Differential Equations (PDEs) is introduced to describe the physical behavior of the proposed problem. With the inclusion of relevant equation variables, this collection of PDEs is transformed into Ordinary Differential Equations (ODEs) which are in a less complex form. Then the bvp4c solver was employed to solve the respective equations. The characteristics of fluid velocity and temperature are investigated graphically. It is found the buoyancy assisting and opposing flows offered dual solutions whereas the purely forced convection flow gives a unique solution. Through an investigation of flow stability, the first solution is confirmed as the physical one. In essence, the volumetric concentration of Cu increases the heat-transferring ability for assisting and opposing flows. The higher suction imposed at the boundary causes a decrease in the heat transfer rate under the shrinking case.

Keywords: Mixed convection; hybrid nanofluid; Eyring-Powell; Riga plate; stagnation point flow.

1. Introduction

Convection refers to the transfer of heat from one place to another by fluid motion. Forced convection occurs when an external source drives fluid motion. However, natural convection occurs when buoyant forces due to density variations alone drive fluid motion. Mixed convection occurs when both forced and natural convection mechanisms are at work. The study of mixed convection flow is essential in various manufacturing processes that involve fluid flow. The presence of dual solutions in computation is a topic of interest among researchers. For example, Merkin [1] investigated the convective flow towards a vertical plate in a porous medium. Merkin [2] discovered dual solutions in his study. Lok et al. [3] observed similar problems for the stagnation micropolar fluid, which led to the extension of this study to the stagnation flow problem. Ishak et al. [4] discovered that non-unique solutions are also possible for the assisting flow as opposed to the opposing flow. Additionally, Subhashini et al. [5], Harris et al. [6], Rosca et al. [7], and Khashi'ie et al. [8, 9] are also working on determining the dual solutions specifically for the case of mixed convection flow.

Over the past several years, plenty of studies have been carried out on the development of enhanced heat transfer fluids. Such fluids like Ethylene glycol, oil, and water are among the regular fluids that are frequently utilized in engineering and manufacturing industries. However, these fluids' delayed heat transfer rate is a result of their poor thermal conductivity. To cover up for this shortcoming, a substance known as "nanofluid" is applied to the fluids in a single nanoparticle. A hybrid nanofluid is then created to improve the standard nanofluid's thermal capabilities. The work by Turcu et al. [10] and Jana et al. [11] were among the pioneers who used hybrid nano-composite particles. Such fluid was an advanced fluid entailing a combination of particles with a base fluid that improvised the rate of heat transfer (Sarkar et al. [12]). According to Devi & Devi [13], Cu-Al₂O₃/water hybrid nanofluids transferred heat more rapidly than the nanofluid (Cu-water) when a magnetic field was utilized (magnetohydrodynamics MHD). The adapted thermophysical parameters described were in exceptional agreement with the previously collected work done by Suresh et al. [14]. They modified the model by Tiwari and Das [15] to include these new thermophysical features. Meanwhile, using a Cu- Al₂O₃/water hybrid nanofluid, Nadeem et al. [16] investigated stagnation flow embedding with thermal slip over a circular

cylinder. A model was also created by Sajid & Ali [17] and Esfe et al. [18] to forecast the conductivity, especially in carbon nanotubes. Thermal materials, field emission, conductive qualities, energy storage, CNT-based molecular electronics and control of thermal conductivity are just some of the possible applications of carbon nanotubes. Due to their high molecular weight, they are virtually impermeable in any known solution (He & Abd Elazem [19]). Alumina and copper are commonly used together in theoretical and practical research on hybrid nanofluids. The irreversibility analysis of Al2O3-water nanofluid flow with changeable characteristics, carried out by Kumar et al. [20], is one of the most recent advances in nanofluids. Muhammad et al. [21] research on hybrid nanoparticles of CuO and CNTs in engine oil, taking into account viscous dissipation. Other scholars, such as Hanafi et al. [22], have further investigated the uses, development, and thermophysical characteristics of hybrid nanofluids.

Research related to heat transfer in fluids has always been of great interest to scientists, especially in discovering ways to enhance them. However, the selection of fluid based on factors such as homogeneity, compressibility, fluid type, and phases plays a crucial role in determining the fluid characteristics. These characteristics become the main properties in preparing the improvised heat transfer rate. Non-Newtonian fluids, such as those that resemble blood or shampoo, cannot be modeled using the Navier-Stokes equations that are related to Newtonian fluids due to their complex equations. Powell-Eyring (1944) has produced some methods for the viscosity relaxation theory of prevalent non-Newtonian fluids. Javed et al. [23] examined the research on an Eyring-Powell fluid's stretching flow. The Keller-box technique was used to numerically develop a locally similar solution. It was found that non-Newtonian characteristics have a greater effect on the velocity magnitude compared to a similar Newtonian fluid. Jalil et al. [24] examined the flow of Eyring-Powell over a moving permeable surface by considering the effects employed the Keller-box method. Ali & Zaib [25] conducted an analytical examination of the model of Eyring-Powell nanofluid over a stretching sheet with convective boundary conditions while the numerical examination was taken care of by Aljabali et al. [26-28]. Additionally, Rashad et al. [29] recently embedded the heat generation and porosity in the flow field.

A magnetic field is an important factor in analyzing the thermophysical properties of fluids. Electromagnetic force can be used to monitor fluid movement in highly conductive fluids. The Riga plate, which is a magnetic bar with alternating electrodes and permanent magnets, can be used as an external constraint to enhance fluid electricity. Gailitis [30] used this type of plate to reduce the hydrodynamic resistance of an electrolyte. Meanwhile, Iqbal et al. [31] employed the Keller-box scheme to assess the effects of stagnation flow on a Riga plate and confirmed the decay of temperature distribution due to melting heat transfer while improvised by the radiative circumstance. Rasool and Zhang [32] studied the second-grade nanofluidic flow across a convectively heated vertical Riga plate, while Nasrin et al. [33] investigated the laminar and incompressible Casson fluid flows over a horizontal Riga plate. Khashi'ie [34, 35] presented a convection hybrid nanofluid flow and stagnation point over a vertical Riga plate with a suction effect. Other valuable investigations of the Riga plate include those by Goud [36] and Akaje [37].

The current study aims to analyze the flow of Eyring-Powell fluid towards a porous Riga plate affected by conveying the hybrid nanofluid. Accordingly, buoyancy assisting and opposing flow regions are explored for dual solutions under suction and EMHD parameters. Water is used as the base fluid along with Cu and Al2O3. The Devi & Devi [13] correlation is used while the Eyring-Powell model is adopted from Javed et al. [23]. The reduced ODEs are then solved by the bvp4c method.

2. Mathematical Model

The Eyring-Powell fluid conveying Cu- Al2O3/ water on the Riga plate is considered as laminar, stable, and incompressible NH as thermal boundary condition where the Riga plate is composed of electrodes with magnets having the same width p, S. N (north) and S (south) represent the magnet's polarity, while the Riga plate's electromagnetic field produces the Lorentz force. Since b is a positive constant, then the free stream velocity is defined by $u_e(x) = bx$. Depending on whether the $x -$ direction is positive or negative, the Lorentz force either assists or opposes the flow. The physical model's assumptions are also addressed. The physical model's assumptions are also addressed. When the mixed convection occurrence is present, the ambient temperature T_∞, is a constant, while the variable wall temperature is $T_w(x) = T_\infty + T_0 x$; T_0 is temperature term that $T_0 > 0$ $(T_w > T_\infty)$ is specified for assisting flow and $T_0 < 0$ $(T_w < T_\infty)$ is for opposing flow. The Riga plate is non-static; hence, stretching/shrinking velocity is treated $u = \varepsilon u_w(x)$.

Under the presumptions outlined above and undergoing boundary layer and Boussinesq approximation, the Cartesian coordinate of the Eyring-Powell hybrid nanofluid with boundary conditions are presented in Eqs. (1) to (4). The idea on the system of equations is adopted from [13, 23, 38].
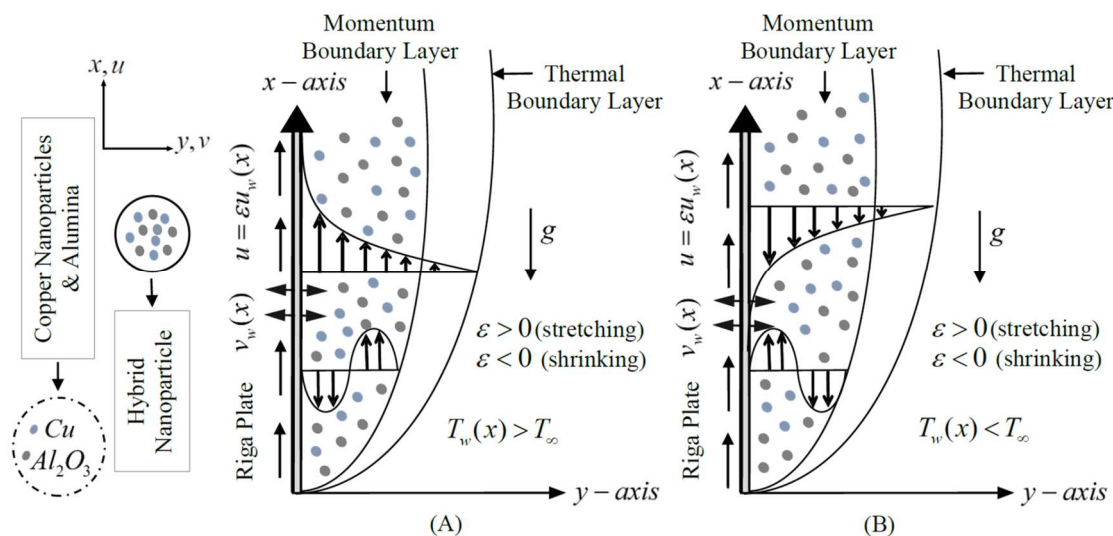

Fig. 1. Physical geometry of flow.

Table 1. Thermophysical of regular and hybrid nanofluids (Takabi and Salehi [39], Tiwari and Das [15], Devi and Devi [13], Rostami et al. [38]).

Properties	Regular Nanofluid	Hybrid Nanofluid
Thermal Conductivity	$\dfrac{k_{nf}}{k_f} = \left(\dfrac{k_s + 2k_f - 2\phi(k_f - k_s)}{k_s + 2k_f + \phi(k_f - k_s)} \right)$	$\dfrac{k_{hnf}}{k_{bf}} = \left(\dfrac{\dfrac{\phi_2 k_{s2} + \phi_1 k_{s1}}{\phi} + 2k_{bf} + 2(\phi_2 k_{s2} + \phi_1 k_{s1}) - 2\phi k_{bf}}{\dfrac{\phi_2 k_{s2} + \phi_1 k_{s1}}{\phi} + 2k_{bf} - (\phi_2 k_{s2} + \phi_1 k_{s1}) + \phi k_{bf}} \right)$
Dynamic Viscosity	$\dfrac{\mu_{nf}}{\mu_f} = \dfrac{1}{(1-\phi)^{2.5}}$	$\dfrac{\mu_{hnf}}{\mu_f} = \dfrac{1}{(1-\phi_1)^{2.5}(1-\phi_2)^{2.5}}$
Electrical Conductivity	$\dfrac{\sigma_{nf}}{\sigma_f} = 1 + \dfrac{3(\sigma-1)\phi}{2+\sigma-(\sigma-1)\phi}$ where $\sigma = \dfrac{\sigma_s}{\sigma_f}$,	$\dfrac{\sigma_{hnf}}{\sigma_{bf}} = \left(\dfrac{\sigma_{s2} + 2\sigma_{bf} - 2\phi_2(\sigma_{bf} - \sigma_{s2})}{\sigma_{s2} + 2\sigma_{bf} + \phi_2(\sigma_{bf} - \sigma_{s2})} \right)$ where $\dfrac{\sigma_{bf}}{\sigma_f} = \left(\dfrac{\sigma_{s1} + 2\sigma_f - 2\phi_1(\sigma_f - \sigma_{s1})}{\sigma_{s1} + 2\sigma_f + \phi_1(\sigma_f - \sigma_{s1})} \right)$
Density	$\rho_{nf} = (1-\phi)\rho_f + \phi\rho_s$	$\rho_{hnf} = (1-\phi)\rho_f + \phi_1\rho_{s1} + \phi_2\rho_{s2}$
Heat Capacity	$(\rho c_p)_{nf} = (1-\phi)(\rho c_p)_f + \phi(\rho c_p)_s$	$(\rho c_p)_{hnf} = (1-\phi)(\rho c_p)_f + \phi_2(\rho c_p)_{s2} + \phi_1(\rho c_p)_{s1}$
Thermal Expansion	$(\rho\beta_T)_{nf} = (1-\phi)(\rho\beta_T)_f + \phi(\rho\beta_T)_s$	$(\rho\beta_T)_{hnf} = (1-\phi)(\rho\beta_T)_f + \phi_2(\rho\beta_T)_{s2} + \phi_1(\rho\beta_T)_{s1}$

Table 2. Thermophysical properties of the base fluid and nanoparticles (Oztop and Abu-Nada [41]).

Thermophysical Properties	Water	Al$_2$O$_3$	Cu
$\rho(kg/m^3)$	997.1	3970	8933
$c_p(J/kgK)$	4179	765	385
$k(W/mK)$	0.6130	40	400
$\beta_T(K^{-1})$	21×10^{-5}	0.85×10^{-5}	1.67×10^{-5}
$\sigma(s/m)$	5.5×10^{-6}	35×10^{6}	59.6×10^{6}

$$\frac{\partial u}{\partial x} + \frac{\partial v}{\partial y} = 0, \tag{1}$$

$$u\frac{\partial u}{\partial x} + v\frac{\partial u}{\partial y} = u_e(x)\frac{du_e(x)}{dx} + \frac{\mu_{hnf}}{\rho_{hnf}}\frac{\partial^2 u}{\partial y^2} + \frac{1}{\rho_{hnf}\tilde{\beta}c^*}\left(\frac{\partial^2 u}{\partial y^2}\right) - \frac{1}{2\rho_{hnf}\tilde{\beta}c^{*3}}\left(\frac{\partial u}{\partial y}\right)^2\frac{\partial^2 u}{\partial y^2} + \frac{(\rho\beta_T)_{hnf}}{\rho_{hnf}}g(T-T_\infty) + \frac{\pi j_0 M_0}{8\rho_{hnf}}e^{-\pi y/p}, \tag{2}$$

$$(\rho c_p)_{hnf}\left(u\frac{\partial T}{\partial x} + v\frac{\partial T}{\partial y}\right) = k_{hnf}\left(\frac{\partial^2 T}{\partial y^2}\right). \tag{3}$$

The associated boundary condition (NH) is as follows:

$$u = \varepsilon u_w(x), \quad v = v_w = -S(bv_f)^{1/2}, \quad T = T_w, \quad -k_{hnf}\frac{\partial T}{\partial y} = h_s T \quad \text{at} \quad y = 0,$$
$$u \to u_e, \quad T \to T_\infty \quad \text{as} \quad y \to \infty. \tag{4}$$

The terms u and v are the velocity in $x-$ and $y-$ directions, respectively. The $x-$ axis is assessed correspondence to the surface, whereas $y-$ axis is upright to it, $\tilde{\beta} = \beta_0 x^{-1}$ and $c^* = c_0 x$ are the parameters referring to Eyring-Powell model, ρ_{hnf} is the density, μ_{hnf} is the dynamic viscosity, $(\rho c_p)_{hnf}$ is the heat capacitance, k_{hnf} is the thermal conductivity, $(\beta_T)_{hnf}$ is the thermal expansion coefficient for hybrid nanofluid, and c_p is the specific heat at constant pressure. In addition, g is gravitational acceleration, $M_0 = M_1 x$ is a magnetic characteristic, while the breadth of magnets as well as electrodes are indicated as p. Moreover, $v_w = -S(a v_f)^{1/2}$ denotes the constant mass velocity while j_0 is current density. The term $S > 0$ links to the suction while $S < 0$ is for injection.

Table 1 summarizes the thermophysical of regular and hybrid nanofluids, where the density, and heat capacity are given by $\rho, \rho c$. The dynamic viscosity, thermal conductivity, and thermal expansion are represented by μ, k, and β_T, respectively. Meanwhile, the subscript terms f, nf, hnf, and s are for the base fluid, nanofluid, hybrid nanofluid, and nanoparticle, respectively, where $s1$ and $s2$ stand for different types of particles. Additionally, ϕ_1 (first particle) and ϕ_2 (second particle) are used to denote the solid volume fractions of nanoparticles. The first nanoparticle in the current work is alumina (Al$_2$O$_3$), the second nanoparticle is copper (Cu), and water is utilized as the fluid's base. Table 2 captures the thermophysical characteristics of the selected nanoparticles and base fluid.

The continuity Eq. (1) is fully satisfied. However, the following relevant similarity transformations is introduced:

$$u = bxf'(\eta), \quad v = -(bv_f)^{1/2}f(\eta), \quad \eta = \left(\frac{b}{v_f}\right)^{1/2}y, \quad \theta(\eta) = \frac{T-T_\infty}{T_w-T_\infty}. \tag{5}$$

Hence, by adopting Eq. (5) to Eqs. (2) to (4), the following ODEs are attained

$$\frac{\mu_{hnf}}{\mu_f} f''' + M f''' - BM f''^2 f''' + \frac{\rho_{hnf}}{\rho_f}(ff'' - f'^2) + \frac{(\rho\beta_T)_{hnf}}{(\rho\beta_T)_f}\lambda\theta + Z e^{-d\eta} + 1 = 0, \tag{6}$$

$$\frac{1}{Pr}\frac{k_{hnf}/k_f}{(\rho c_p)_{hnf}/(\rho c_p)_f}\theta'' + f\theta' - f'\theta = 0. \tag{7}$$

The simplified boundary condition is as follows:

$$f(0) = S, \quad f'(0) = \varepsilon, \quad -\frac{k_{hnf}}{k_f}\theta'(0) = \gamma(1+\theta(0)) \ \text{(NH)}, \quad \text{at } \eta = 0$$

$$f'(\eta) \to 1, \qquad \theta(\eta) \to 0 \qquad \text{as } \eta \to \infty. \tag{8}$$

where the fluid parameters are $M = 1/\mu_f\tilde{\beta}c^*$ and $B = a^3/2c_0^2 v_f$. The term $\lambda = Gr/Re_x^2$ refers to the mixed convection. The quantities of $\lambda > 0$ is analogous to assisting flow, $\lambda < 0$ is equivalent to the opposing flow, and $\lambda = 0$ denotes the pure forced convective flow. Furthermore, $Gr = g(\beta_T)_f(T_w(x) - T_\infty)x^3/v_f^2$ is the Grashof number and $Re_x = bx^2/v_f$ is the local Reynolds number based on the elongated velocity, $u_e(x) = bx$. Additionally, $Z = \pi j_0 M_1/8b^2\rho_f$ defines the modified Hartmann number at which the $Z > 0$ signifies the intensity of assisting flow (x − direction) (Khashi'ie et al. [9, 34] and Ahmad [40]). $d = \pi\sqrt{v_f/b}/p$ is correlated with the width of magnets and electrodes, while the Prandtl number is represented by $Pr = (c_p\mu)_f/k_f$ and $\gamma = -h_s\sqrt{v_f/a}$ is the conjugate parameter.

The skin friction coefficient C_f and the local Nusselt number Nu_x are:

$$C_f = \frac{\tau_w}{\rho_f u_e^2(x)}, \qquad Nu_x = \frac{xq_w}{k_f(T_w(x) - T_\infty)}, \tag{9}$$

where $\tau_w = \left(\mu_{hnf} + \frac{1}{\tilde{\beta}c^*}\right)\frac{\partial u}{\partial y} - \frac{1}{6\tilde{\beta}}\left(\frac{1}{c^*}\frac{\partial u}{\partial y}\right)^3$ specifies the shear stress, while $q_w = -k_{hnf}\left(\frac{\partial T}{\partial y}\right)_{y=0}$ is the surface heat flux. The quantities of reduced skin friction and local Nusselt are:

$$C_f Re_x^{1/2} = \frac{\mu_{hnf}}{\mu_f} f''(0) + M f''(0) - \frac{B}{3}M f''^3(0), \qquad Nu_x Re_x^{-1/2} = -\frac{k_{hnf}}{k_f}\gamma\left(1 + \frac{1}{\theta(0)}\right). \tag{10}$$

3. Stability Analysis

To determine the stable solutions, the scrutiny of flow stability is decisive. Equations (6) and (7) subject to Eq. (8) produce similar solutions. Salleh et al. [42] discussed the stability of nanofluids in detail. Following Merkin's research [2], the unsteady case is originally viewed as:

$$\frac{\partial u}{\partial t} + u\frac{\partial u}{\partial x} + v\frac{\partial u}{\partial y} = u_e(x)\frac{du_e(x)}{dx} + \frac{\mu_{hnf}}{\rho_{hnf}}\frac{\partial^2 u}{\partial y^2} + \frac{1}{\rho_{hnf}\tilde{\beta}c^*}\left(\frac{\partial^2 u}{\partial y^2}\right) - \frac{1}{2\rho_{hnf}\tilde{\beta}c^{*3}}\left(\frac{\partial u}{\partial y}\right)^2\frac{\partial^2 u}{\partial y^2} + \frac{(\rho\beta_T)_{hnf}}{\rho_{hnf}}g(T - T_\infty) + \frac{\pi j_0 M_0}{8\rho_{hnf}}e^{-\pi y/p}, \tag{11}$$

$$(\rho c_p)_{hnf}\left(\frac{\partial T}{\partial t} + u\frac{\partial T}{\partial x} + v\frac{\partial T}{\partial y}\right) = k_{hnf}\left(\frac{\partial^2 T}{\partial y^2}\right). \tag{12}$$

The time variable transformation ($\tau = bt$) yields:

$$\eta = \left(\frac{b}{v_f L}\right)^{1/2} y, \quad \psi = (bv_f)^{1/2} x f(\eta, \tau), \quad \theta(\eta, \tau) = \frac{T - T_\infty}{T_w(x) - T_\infty}\text{(NH)},$$

$$u = bx\frac{\partial f}{\partial \eta}(\eta, \tau), \quad v = -(bv_f)^{1/2} f(\eta, \tau). \tag{13}$$

and attained the following equation:

$$\frac{\mu_{hnf}}{\mu_f}\frac{\partial^3 f}{\partial \eta^3} + M\frac{\partial^3 f}{\partial \eta^3} - BM\left(\frac{\partial^2 f}{\partial \eta^2}\right)^2\frac{\partial^3 f}{\partial \eta^3} + \frac{\rho_{hnf}}{\rho_f}\left(f\frac{\partial^2 f}{\partial \eta^2} - \left(\frac{\partial f}{\partial \eta}\right)^2\right) + \frac{(\rho\beta_T)_{hnf}}{(\rho\beta_T)_f}\lambda\theta - \frac{\rho_{hnf}}{\rho_f}\left(\frac{\partial^2 f}{\partial \eta\partial\tau}\right) + Z e^{-d\eta} + 1 = 0, \tag{14}$$

$$\frac{1}{Pr}\frac{k_{hnf}/k_f}{(\rho c_p)_{hnf}/(\rho c_p)_f}\frac{\partial^2\theta}{\partial \eta^2} + f\frac{\partial\theta}{\partial \eta} - \frac{\partial f}{\partial \eta}\theta - \frac{\partial\theta}{\partial \tau} = 0. \tag{15}$$

subjected to:

$$f(0,\tau) = S, \quad \frac{\partial f}{\partial \eta}(0,\tau) = \varepsilon, \quad -\frac{k_{hnf}}{k_f}\frac{\partial\theta}{\partial \eta}(0,\tau) = \gamma(1+\theta(0,\tau)) \ \text{(NH)}, \quad \text{at } \eta = 0$$

$$\frac{\partial f}{\partial \eta}(\eta,\tau) \to 1, \qquad \theta(\eta,\tau) \to 0 \qquad \text{as } \eta \to \infty. \tag{16}$$

Table 3. Numerical $f''(0)$ values at $\eta_\infty = 20$, $\varepsilon = 1$, $Z = d = 0.5$ and Pr = 5.

Existing Literature	Model	Boundary Condition	Limiting Cases	Value of $f''(0)$
Present Study (bvp4c solution)	$\frac{\mu_{hnf}}{\mu_f} f''' + M f''' - BM(f'')^2 f'''$ $+ \frac{\rho_{hnf}}{\rho_f}(ff'' - f'^2) + \frac{(\rho\beta_T)_{hnf}}{(\rho\beta_T)_f}\lambda\theta + ze^{-d\eta} + 1 = 0.$	$f(0) = S$ $f'(0) = \varepsilon$ $f'(\infty) = 0$	$B = M = 0$ $\phi_1 = \phi_2 = 0$ $S = \lambda = 0$	1.53946
Ahmad et al. [40] (shooting and bvp4c solution)	$f''' + ff'' - f'^2 + \lambda(\theta - N_t f) + ze^{-d\eta} + 1 = 0.$	$f(0) = 0$ $f'(0) = 1$ $f'(\infty) = 0$	$\phi_1 = \phi_2 = 0$ $S = \lambda = 0$	1.53947
Khashi'ie [9] (bvp4c solution)	$\left(\frac{\mu_{hnf}/\mu_f}{\rho_{hnf}/\rho_f}\right)\frac{\mu_{hnf}}{\mu_f} f'' + ff'' - f'^2$ $+ \left(\frac{(\rho\beta_T)_{hnf}/(\rho\beta_T)_f}{\rho_{hnf}/\rho_f}\right)\lambda\theta + \left(\frac{z}{\rho_{hnf}/\rho_f}\right)e^{-d\eta} + 1 = 0.$	$f(0) = S$ $f'(0) = \varepsilon$ $f'(\infty) = 0$	$\phi_1 = \phi_2 = 0$ $\varepsilon = 1, S = 0$	1.53947

Table 4. Comparative study of $f''(0)$ when $M, B = Z = d = S = \lambda = \phi_{11} = \phi_{12} = 0$ for various values ε.

ε	Rosca et al. [43] (Keller box)		Present (bvp4c)	
	First Sol.	Second Sol.	First Sol.	Second Sol.
-1.20	0.932473	0.233649	0.932457	0.233638
-1.15	1.082231	0.116702	1.082230	0.116700
-1.00	1.328816	0.000000	1.328809	0.000000
0.00	1.232587	-	1.232578	-
0.50	0.713294	-	0.713286	-
1.00	0.000000	-	0.000000	-

Table 5. Comparison values of $C_f \text{Re}_x^{1/2}$ when $Z = d = S = \lambda = \phi_{11} = \phi_{12} = 0$, and $\varepsilon = 1$ (stretching case) for numerous M and B.

M	Javed et al. [23] (Keller box)			Present (bvp4c solution)		
	B = 0	B = 0.2	B = 0.4	B = 0	B = 0.2	B = 0.4
0	-1.0000	-1.0954	-1.1832	-1.0000	-1.0954	-1.1832
0.1	-1.0000	-1.0924	-1.1784	-1.0000	-1.0924	-1.1784
0.4	-1.0000	-1.0894	-1.1735	-1.0000	-1.0893	-1.1734

Using the perturbation $f(\eta,\tau) = f_0(\eta) + e^{-\gamma_0\tau}F(\eta)$, $\theta(\eta,\tau) = \theta_0(\eta) + e^{-\gamma_0\tau}G(\eta)$, the linearized eigenvalue equations relevant to the problem are:

$$\frac{\mu_{hnf}}{\mu_f}F''' + MF''' - BMf_0''^2 F''' - 2BMf_0''f_0'''F'' + \frac{\rho_{hnf}}{\rho_f}\left(f_0F'' - 2f_0'F' + \gamma_0F' + f_0''F\right) + \frac{(\rho\beta_T)_{hnf}}{(\rho\beta_T)_f}\lambda G = 0, \tag{17}$$

$$\frac{1}{\text{Pr}}\frac{k_{hnf}/k_f}{(\rho c_p)_{hnf}/(\rho c_p)_f}G'' + f_0G' + F\theta_0' - f_0'G - F'\theta_0 + \gamma_0G = 0. \tag{18}$$

Nonetheless, the linearized condition in Eq. (19) is used for this problem:

$$F(0) = 0, \ F'(0) = 0, \ F''(0) = 1(\text{replaced}), \ G(0) = 0,$$
$$F'(\eta) \to 0 (\text{relaxed}), \ G(\eta) \to 0 \ \text{at} \ \eta \to \infty. \tag{19}$$

The resulting eigenvalue will determine the type of solution (real or unreal).

4. Results and Discussion

The formulations of the problems were constructed mathematically and solved using the bvp4c solver; the similarity solutions are obtained by solving Eqs. (6) to (8). The values $\eta_\infty = 20$, $\phi_1 = 0.1$ and Pr = 6.2 are considered constant for the entire computation. The error tolerance is set as 10^{-10}. As it goes on, the quantity of volume fraction (copper) and values of parameter fluid, EMHD, mixed convection, and stretching/shrinking, are chosen appropriately. However, it is necessary to select the initial guesses to suit the values of the parameters involved to demonstrate the effectiveness of the results.

A direct comparison was made on the Riga plate surface between the output documented by Ahmad et al. [40] (two-phase nanofluid, permeable ($v = v_w$), static ($u = 0$), shooting method, and bvp4c solver) and Khashi'ie [9] (one-phase hybrid nanofluid; impermeable ($v = 0$); static ($u = 0$); bvp4c solver), as well as those of the current study (one-phase hybrid nanofluid; stretching/shrinking plate ($u = \varepsilon u_w$); bvp4c solver). Table 3 shows a strong agreement between the present model with the established outputs. Tables 4 and 5 present the reduced non-Newtonian Eyring- Powell model with Javed et al. [23] and compare the values from Rosca et al. [43], considering the stretching/shrinking case when $Z = d = 0$ (flat plate without EMHD), $S = 0$ (impermeable), $\lambda = 0$ (pure forced convective flow), $\phi_1 = \phi_{12} = 0$ (pure water), and $M, B = 0$.

Table 6. $Nu_x \, Re_x^{-1/2}$ values when $\phi_1 = 0.1$, $\gamma = 1$, $Z = d = 0.5$, $B = M = 0.1$, $S = 0, 0.3$ for different λ ([ ] indicates the second solution).

λ	S	ϕ_2		
		0.05	0.1	0.3
-0.5	0	1.673318	1.683598	1.966838
		[-2.043318]	[-2.113405]	[-2.353237]
	0.3	2.777521	3.029818	3.23234
		[-7.113018]	[-7.344355]	[-8.034972]
0.005	0	1.698420	1.709531	2.077141
		[5.113014]	[5.353611]	[6.041009]
	0.3	3.007596	3.029818	3.23234
		[9.333603]	[9.695550]	[10.472857]
0.5	0	1.782474	1.954562	2.141140
		[4.592103]	[4.903567]	[5.671205]
	0.3	3.816182	3.836115	4.053732
		[8.330176]	[8.710000]	[9.481147]
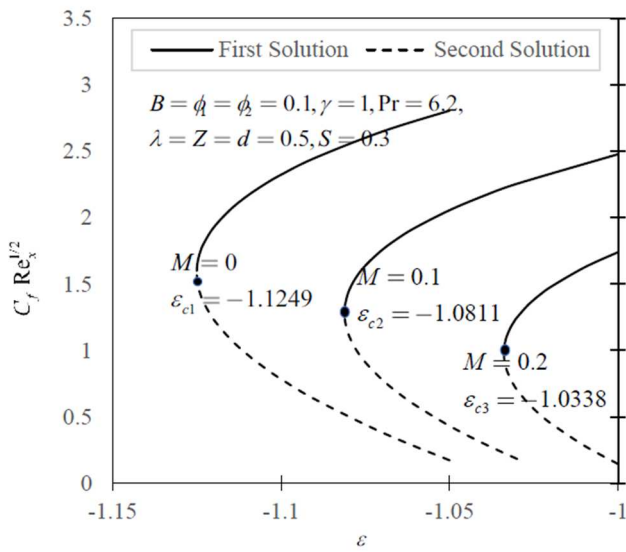
Fig. 2. Variations of $C_f \, Re_x^{1/2}$ for various M.
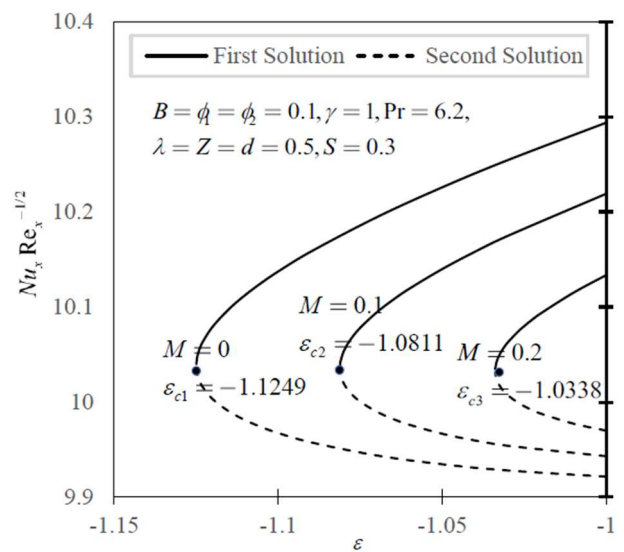
Fig. 3. Variations of $Nu_x \, Re_x^{-1/2}$ for various M.
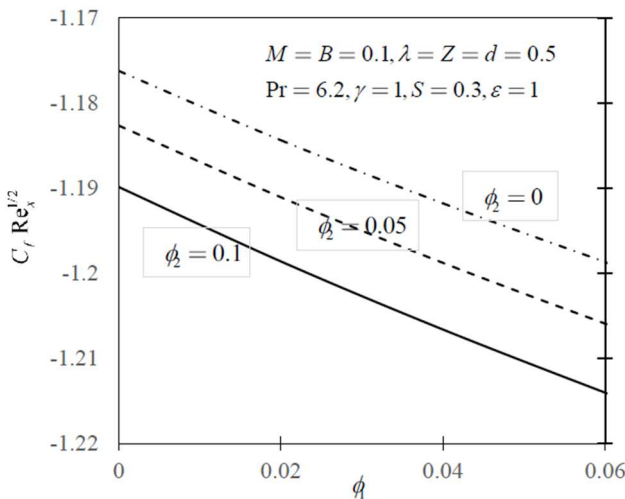
Fig. 4. Variations of $C_f \, Re_x^{1/2}$ for various ϕ_2.
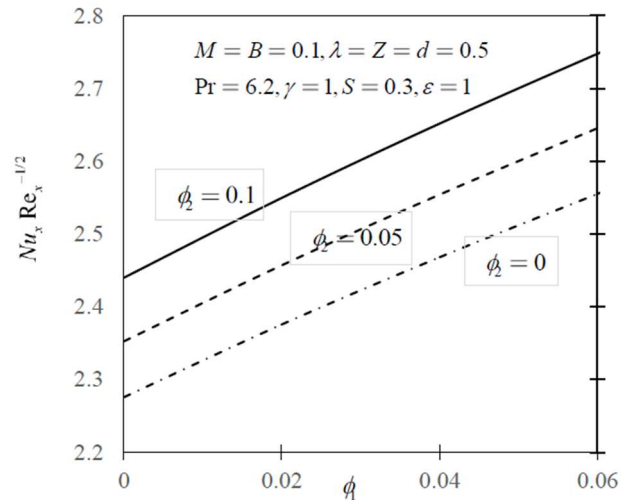
Fig. 5. Variations of $Nu_x \, Re_x^{-1/2}$ for various ϕ_2.

Table 6 shows that, for both flow instances, two solutions are possible where the first solution offered a better heat transfer rate. In reality, the assisting flow has a wall temperature that is greater than the fluid temperature. This shows the transferring of heat takes place direct from wall while the opposing flow has a negative impact. As a result, it can be deduced that an assisting flow always transfers more heat than an opposing flow. Based on the current observation, the greater amount of ϕ_2 increases heat transfer rate for $S = 0$ and $S = 0.3$.
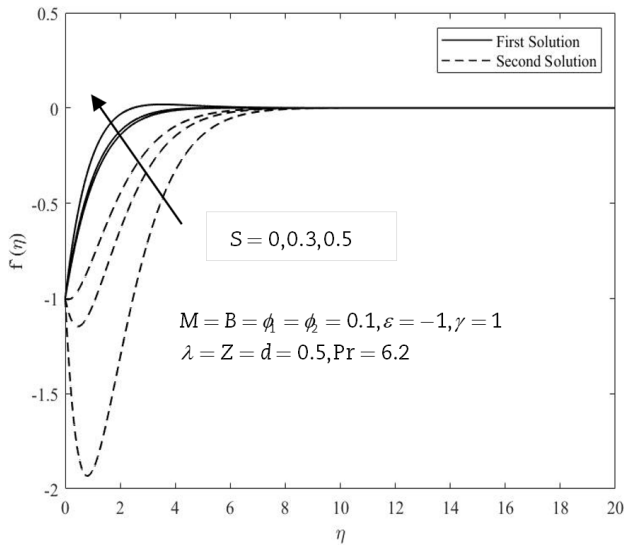
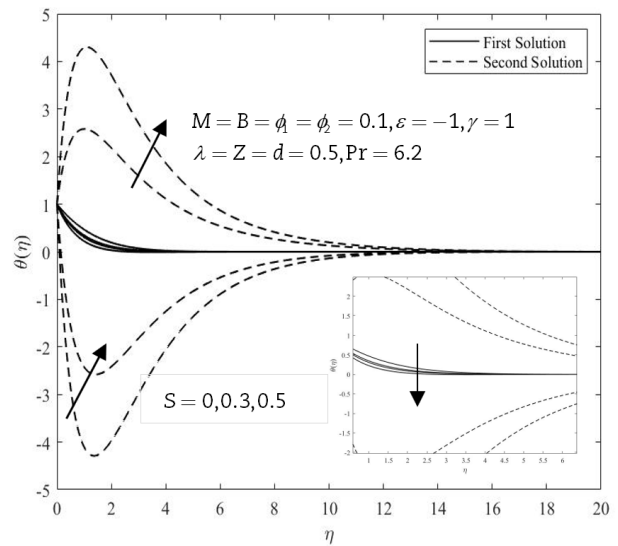**Fig. 6.** Variations of $f'(\eta)$ for various λ.

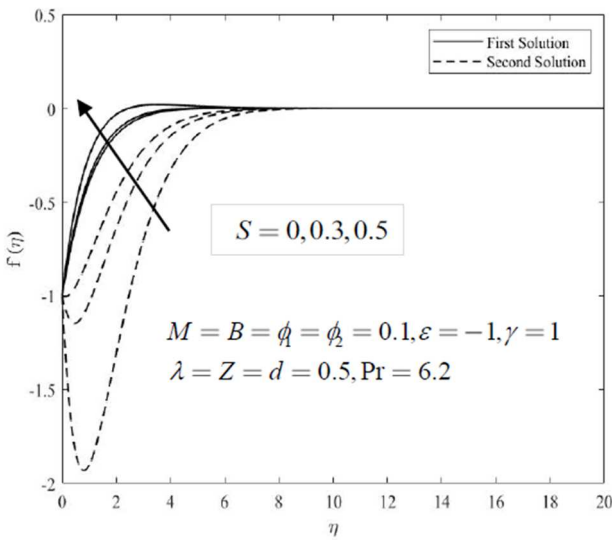**Fig. 7.** Variations of $\theta(\eta)$ for various λ.

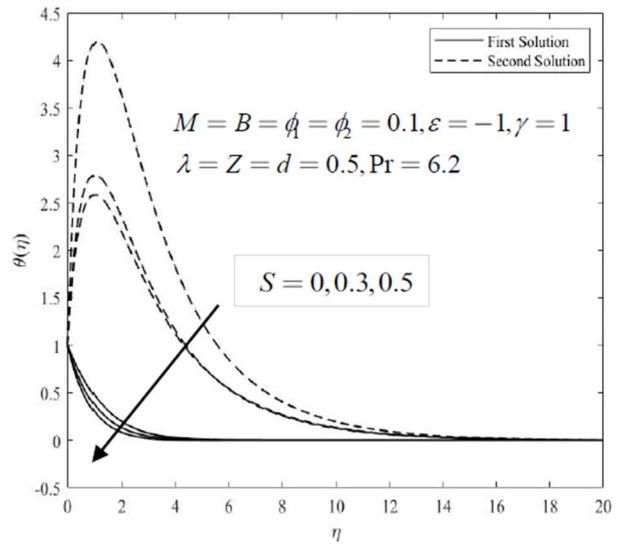**Fig. 8.** Variations of $f'(\eta)$ for various S.

Fig. 9. Variations of $\theta(\eta)$ for various S.

Figures 2 and 3 display the graph of skin friction and the Nusselt number concerning the fluid parameter, M, in the shrinking environment. Evidently, when M increases, $C_f \operatorname{Re}_x^{1/2}$ values decrease and $Nu_x \operatorname{Re}_x^{-1/2}$ contributions increase. Physically, the greater values of M produce obstacles that slow down the rate of shear-thinning and reduce the attachment between fluid and surfaces, thus generating a small drag. However, the increase in ε significantly boosts the values of $C_f \operatorname{Re}_x^{1/2}$. For $M=0$, on the other hand, it is observed that the value of $C_f \operatorname{Re}_x^{1/2}$ only increases to a certain value of ε and thereafter exhibits a declining trend. Additionally, the dual $C_f \operatorname{Re}_x^{1/2}$ and $Nu_x \operatorname{Re}_x^{-1/2}$ solutions reach a certain critical level of ε. The critical values also reach up to $\varepsilon_{c1} = -1.1249$, $\varepsilon_{c2} = -1.0811$ and $\varepsilon_{c3} = -1.0338$ for $M = 0, 0.1, 0.2$, respectively. Nevertheless, no other solutions have been achieved beyond the above-mentioned critical values.

The graph of $C_f \operatorname{Re}_x^{1/2}$, and $Nu_x \operatorname{Re}_x^{-1/2}$ for ϕ_1 and various values of ϕ_2 are highlighted in Figs. 4 and 5. The improvement of ϕ_2 and ϕ_1 results in increasing heat transport. For these figures, the sheet is assumed to be stretching ($\varepsilon = 1$), and it is clear that at constant ϕ_1, the value of $C_f \operatorname{Re}_x^{1/2}$ decreases with a greater value of ϕ_2 but behaves inconsistently in $Nu_x \operatorname{Re}_x^{-1/2}$. Notably, the presence of significant ϕ_1 decreases the value of $C_f \operatorname{Re}_x^{1/2}$ while enhancing $Nu_x \operatorname{Re}_x^{-1/2}$. Alternatively, the fluid devoid of nanoparticles ($\phi_1 = \phi_{12} = 0$) has been discovered to provide a greater value of $C_f \operatorname{Re}_x^{1/2}$ and a lower value of $Nu_x \operatorname{Re}_x^{-1/2}$ than the fluid that includes nanoparticles. The results show the presence of Cu and Al2O3 nanoparticles has a substantial influence on the fluid properties. Physically, the drag force decreases as the concentration grows. As a result, the concentration of nanoparticles resisted the drag force, led to lowering skin friction. The base fluid's enhanced thermal conductivity is also influenced by the rising nanoparticle concentration. Additionally, the fluid flow's particles impacting with one another lose energy at a faster pace and raise the ambient temperature. In comparison to conventional nanofluids (single particles), it is well-expected the heat transference of hybrid nanofluids will increase exponentially.

Figures 6 to 9 demonstrate the velocity and temperature distribution under different λ and S. The asymptotic fulfillment of the far field boundary condition by all profiles validates the accuracy of the current solutions. The increase in λ (from opposing to assisting flow) lead to lessening temperature and enhance in fluid's velocity. The fluid velocity is increased due to extra kinetic energy compare to opposing flow. While the temperature profile shows the opposite trend, both the first and second solutions increase as suction develop. Suction builds the flow neighboring to the Riga plate by reducing the width of the momentum boundary

layer. Furthermore, the bvp4c solver is used to resolve the linearized eigenvalue problem in Eqs. (17) to (19). The flow stability improves under initial drop of disturbance in time; if $\gamma_0 > 0,$ then this phenomenon occurs. Expected from initial development of the disturbance with time $(e^{-\gamma_0 \tau} \to \infty$ as $\gamma_0 < 0$ and $\tau \to \infty)$, the flow is unstable under $\gamma_0 < 0$. As can be seen in Fig. 10, the quantities of γ_0 are positive on first solutions on the upper branch; however, the values become negative for the second solutions on the lower branch. Additionally, when $\varepsilon \to \varepsilon_c$ occurs, the γ_0 values for both branches get nearer zero. This result indicates that, in contrast to the second solution, the physically stable outcome lies on the first solution. Besides, it is assumed that the bifurcation of solutions occurs at $\varepsilon = \varepsilon_c$.
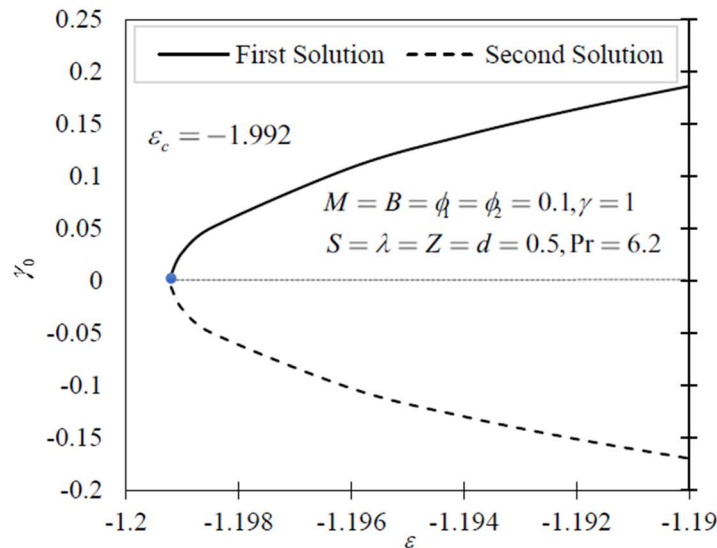

Fig. 10. Smallest eigenvalues (γ_0) of first and second solutions toward ε.

The way forward for this research is to apply the theory of conservation laws in fractal space. This is because such laws will give the new physical insight to the particles of fluid flow. One of the theories in fractal space is two-scale fractal theory which able in analyzing the systems exhibiting the fractal properties for microscale as well as macroscale. Since the nanofluid containing the particles which will significantly enhance the fluid properties, understanding its complex interactions at multiple scales able to bring new knowledge to the flow field. Incorporating the fractal elements in Navier Stokes equation need details investigation since its formulation involve the emphasizing of scale-invariant structures. Embedding the fractal geometry and fractional calculus in modelling able to improvise the accuracy of develop models demonstrating the complex fluid systems which crucial engineering and industrial applications. The discussion on this topic was also documented in [44].

5. Conclusions

The current investigation focused on the flow over a permeable stretching/shrinking Riga plate of Eyring-Powell with Cu-Al_2O_3/water driven by buoyancy. The conclusions are as follows:

- Cu-Al_2O_3/water on Eyring-Powell fluid exhibits improved thermal conductivity.
- In comparison to pure water and the alumina-water nanofluid, the composition of Cu-Al_2O_3/water exhibits a higher skin friction coefficient and heat transfer rate.
- The dual solutions are achieved on assisting and the opposing flow cases in a given range of the buoyancy parameter, and the region of the opposing flow is where the separation point is situated.
- For the assisting flow situation compared to the opposing flow situation, the reduced skin friction coefficient and heat transfer rate are greater.
- The improvement of the suction and mixed convection parameters results in an increase in the velocity profile and a decline in the temperature profile.
- For both assisting and opposing buoyancy flows, an upsurge in Cu volumetric concentration, suction, and EMHD parameters increases the heat transfer rate.
- The upper branch (first solution) is stable, according to the stability study, but the lower branch (second) solution is not.

Author Contributions

A. Aljabali prepared the research conceptualization, developed the research methodology, conducted the formal analysis, and write the original draft; A.R.M. Kasim prepared the research conceptualization, validate the findings, reviewed, and edited the writing and provided supervision; N.S. Khashi'ie and I. Waini developed the methodology, utilized the software; N.A.N. Ariffin reviewed and edited the manuscript.

Conflict of Interest

The authors declared no potential conflicts of interest concerning the research, authorship, and publication of this article.

Funding

Data Availability Statements

The datasets generated and/or analyzed during the current study are available from the corresponding author on reasonable request.

References

[1] Merkin, J.H., Mixed convection boundary layer flow on a vertical surface in a saturated porous medium, *Journal of Engineering Mathematics*, 14(4), 1980, 301-313.

[2] Merkin, J.H., On dual solutions occurring in mixed convection in a porous medium, *Journal of Engineering Mathematics*, 20(2), 1986, 171-179.

[3] Lok, Y.Y., Amin, N., Campean, D., Pop, I., Steady mixed convection flow of a micropolar fluid near the stagnation point on a vertical surface, *International Journal of Numerical Methods for Heat & Fluid Flow*, 15(7), 2005, 654-670.

[4] Ishak, A., Nazar, R., Arifin, N.M., Pop, I., Dual solutions in mixed convection flow near a stagnation point on a vertical porous plate, *International Journal of Thermal Sciences*, 47(4), 2008, 417-422.

[5] Subhashini, S.V., Samuel, N., Pop, I., Effects of buoyancy assisting and opposing flows on mixed convection boundary layer flow over a permeable vertical surface, *International Communications in Heat and Mass Transfer*, 38(4), 2011, 499-503.

[6] Harris, S.D., Ingham, D.B., Pop, I., Mixed convection boundary-layer flow near the stagnation point on a vertical surface in a porous medium: Brinkman model with slip, *Transport in Porous Media*, 77, 2009, 267–285.

[7] Rosca, A.V., Rosca, N.C., Pop, I., Note on dual solutions for the mixed convection boundary layer flow close to the lower stagnation point of a horizontal circular cylinder: Case of constant surface heat flux, *Sains Malaysiana*, 43(8), 2014, 1239-1247.

[8] Khashi'ie, N.S., Arifin, N.M., Rashidi, M.M., Hafidzuddin, E.H., Wahi, N., Magnetohydrodynamics (MHD) stagnation point flow past a shrinking/stretching surface with double stratification effect in a porous medium, *Journal of Thermal Analysis and Calorimetry*, 139, 2020, 3635-3648.

[9] Khashi'ie, N.S., Md Arifin, N., Pop, I., Mixed convective stagnation point flow towards a vertical Riga plate in hybrid Cu-Al2O3/water nanofluid, *Mathematics*, 8(6), 2020, 912.

[10] Turcu, R., Darabont, A.L., Nan, A., Aldea, N., Macovei, D., Bica, D., ..., Biro, L.P. New polypyrrole-multiwall carbon nanotubes hybrid materials, *Journal of Optoelectronics and Advanced Materials*, 8(2), 2006, 643-647.

[11] Jana, S., Salehi-Khojin, A., Zhong, W.H., Enhancement of fluid thermal conductivity by the addition of single and hybrid nano-additives, *Thermochimica Acta*, 462(1-2), 2007, 45-55.

[12] Sarkar, J., Ghosh, P., Adil, A., A review on hybrid nanofluids: recent research, development and applications, *Renewable and Sustainable Energy Reviews*, 43, 2015, 164-177.

[13] Devi, S.A., Devi, S.S.U., Numerical investigation of hydromagnetic hybrid Cu–Al2O3/water nanofluid flow over a permeable stretching sheet with suction, *International Journal of Nonlinear Sciences and Numerical Simulation*, 17(5), 2016, 249-257.

[14] Suresh, S., Venkitaraj, K.P., Selvakumar, P., Chandrasekar, M., Synthesis of Al2O3–Cu/water hybrid nanofluids using two step method and its thermo physical properties, *Colloids and Surfaces A: Physicochemical and Engineering Aspects*, 388(1-3), 2011, 41-48.

[15] Tiwari, R.K., Das, M.K., Heat transfer augmentation in a two-sided lid-driven differentially heated square cavity utilizing nanofluids, *International Journal of heat and Mass Transfer*, 50(9-10), 2007, 2002-2018.

[16] Nadeem, S., Abbas, N., Khan, A.U., Characteristics of three-dimensional stagnation point flow of Hybrid nanofluid past a circular cylinder, *Results in Physics*, 8, 2018, 829-835.

[17] Sajid, M.U., Ali, H.M., Thermal conductivity of hybrid nanofluids: a critical review, *International Journal of Heat and Mass Transfer*, 126, 2018, 211-234.

[18] Esfe, M.H., Amiri, M.K., Alirezaie, A., Thermal conductivity of a hybrid nanofluid, *Journal of Thermal Analysis and Calorimetry*, 134(2), 2018, 1113-1122.

[19] He, J.H., Abd Elazem, N.Y., The carbon nanotube-embedded boundary layer theory for energy harvesting, *Facta Universitatis, Series: Mechanical Engineering*, 20(2), 2022, 211-235.

[20] Kumar, K., Chauhan, P.R., Kumar, R., Bharj, R.S., Irreversibility analysis in Al2O3-water nanofluid flow with variable property, *Facta Universitatis, Series: Mechanical Engineering*, 20(3), 2022, 503-518.

[21] Muhammad, K., Hayat, T., Alsaedi, A., Asghar, S., Stagnation point flow of basefluid (gasoline oil), nanomaterial (CNTs) and hybrid nanomaterial (CNTs+ CuO): a comparative study, *Materials Research Express*, 6(10), 2019, 105003.

[22] Hanafi, N.S.M., Ghopa, W.A.W., Zulkifli, R., Sabri, M.A.M., Zamri, W.F.H.W., Ahmad, M.I.M., Mathematical formulation of Al2O3-Cu/water hybrid nanofluid performance in jet impingement cooling, *Energy Reports*, 9, 2023, 435-446.

[23] Javed, T., Ali, N., Abbas, Z., Sajid, M., Flow of an Eyring-Powell non-Newtonian fluid over a stretching sheet, *Chemical Engineering Communications*, 200(3), 2013, 327-336.

[24] Jalil, M., Asghar, S., Imran, S.M., Self-similar solutions for the flow and heat transfer of Powell-Eyring fluid over a moving surface in a parallel free stream, *International Journal of Heat and Mass Transfer*, 65, 2013, 73-79.

[25] Ali, F., Zaib, A., Stagnation point flow on an Eyring-Powell of nanofluid over a stretched surface with convected boundary condition, *International Conference on Computing, Mathematics and Engineering Technologies*, 2019.

[26] Aljabali, A., Kasim, A.R.M., Arifin, N.S., Isa, S.M., Mixed convection of non-Newtonian Eyring-Powell fluid with temperature-dependent viscosity over a vertically stretched surface, *CMC-Computers Materials & Continua*, 66(1), 2021, 421-435.

[27] Aljabali, A., Kasim, A.R.M., Arifin, N.S., Isa, S.M., Ariffin, N.A.N., Analysis of convective transport of temperature-dependent viscosity for non-Newtonian Erying-Powell fluid: A numerical approach, *CMC-Computers Materials & Continua*, 66(1), 2021, 675-689.

[28] Aljabali, A., Mohd Kasim, A.R., Arifin, N.S., Ariffin, N.A.N., Ling Chuan Ching, D., Waini, I., Khashi'ie, N.S., Zainal, N.A., Two-Phase Flow of Eyring–Powell Fluid with Temperature Dependent Viscosity over a Vertical Stretching Sheet, *Mathematics*, 10(17), 2022, 3111.

[29] Rashad, A.M., Nafe, M.A., Eisa, D.A., Heat generation and thermal radiation impacts on flow of magnetic Eyring–Powell hybrid nanofluid in a porous medium, *Arabian Journal for Science and Engineering*, 48(1), 2023, 939-952.

[30] Gailitis, A., On a possibility to reduce the hydrodynamical resistance of a plate in an electrolyte, *Appl. Magnetohydrodyn*, 12, 1961, 143-146.

[31] Iqbal, Z., Azhar, E., Mehmood, Z., Maraj, E.N., Melting heat transport of nanofluidic problem over a Riga plate with erratic thickness: Use of Keller Box scheme, *Results in Physics*, 7, 2017, 3648-3658.

[32] Rasool, G., Zhang, T., Characteristics of chemical reaction and convective boundary conditions in Powell-Eyring nanofluid flow along a radiative Riga plate, *Heliyon*, 5(4), 2019, e01479.

[33] Nasrin, S., Mondal, R.N., Alam, M.M., Impulsively started horizontal Riga plate embedded in unsteady Casson fluid flow with rotation, *Journal of Applied Mathematics and Physics*, 8(9), 2020, 1861-1876.

[34] Khashi'ie, N.S., Arifin, N.M., Pop, I., Wahid, N.S., Effect of suction on the stagnation point flow of hybrid nanofluid toward a permeable and vertical Riga plate, *Heat Transfer*, 50(2), 2021, 1895-1910.

[35] Khashi'ie, N.S., Waini, I., Wahid, N.S., Arifin, N.M., Pop, I., Unsteady separated stagnation point flow due to an EMHD Riga plate with heat generation in hybrid nanofluid, *Chinese Journal of Physics*, 81, 2023, 181-192.

[36] Goud, B.S., Reddy, Y.D., Alshehri, N.A., Jamshed, W., Safdar, R., Eid, M.R., Bouazizi, M.L., Numerical case study of chemical reaction impact on MHD

micropolar fluid flow past over a vertical riga plate, *Materials*, 15(12), 2022, 4060.

[37] Akaje, T.W., Taiwo, M.A., Olajuwon, B.I., Raj, M.T., Akinleye, S.A., Double-Diffusive Nonlinear Buoyancy Force Significance on Free Convective Chemically Reacting Fluids Flow Past Vertical Riga Surface, *Journal of Advanced Research in Fluid Mechanics and Thermal Sciences*, 105(1), 2023, 59-75.

[38] Rostami, M.N., Dinarvand, S., Pop, I., Dual solutions for mixed convective stagnation-point flow of an aqueous silica–alumina hybrid nanofluid, *Chinese Journal of Physics*, 56(5), 2018, 2465-2478.

[39] Takabi, B., Salehi, S., Augmentation of the heat transfer performance of a sinusoidal corrugated enclosure by employing hybrid nanofluid, *Advances in Mechanical Engineering*, 6, 2014, 147059.

[40] Ahmad, R., Mustafa, M., Turkyilmazoglu, M., Buoyancy effects on nanofluid flow past a convectively heated vertical Riga-plate: A numerical study, *International Journal of Heat and Mass Transfer*, 111, 2017, 827-835.

[41] Oztop, H.F., Abu-Nada, E., Numerical study of natural convection in partially heated rectangular enclosures filled with nanofluids, *International Journal of Heat and Fluid Flow*, 29(5), 2008, 1326-1336.

[42] Salleh, S.N.A., Bachok, N., Arifin, N.M., Ali, F.M., Pop, I., Stability analysis of mixed convection flow towards a moving thin needle in nanofluid, *Applied Sciences*, 8(6), 2018, 842.

[43] Rosca, A.V., Rosca, N.C., Pop, I., Numerical simulation of the stagnation point flow past a permeable stretching/shrinking sheet with convective boundary condition and heat generation, *International Journal of Numerical Methods for Heat & Fluid Flow*, 26(1), 2016, 348-364.

[44] Li, X., A fractal-fractional model for complex fluid-flow with nanoparticles, *Thermal Science*, 27(3A), 2023, 2057-2063.

ORCID iD

Ahlam Aljabali https://orcid.org/0009-0006-2382-2332
Abdul Rahman Mohd Kasim https://orcid.org/0000-0001-9359-428X
Najiyah Safwa Khashi'ie https://orcid.org/0000-0002-9092-8288
Iskandar Waini https://orcid.org/0000-0002-9883-5473
Noor Amalina Nisa Ariffin https://orcid.org/0000-0002-7108-1157

Publisher's Note Shahid Chamran University of Ahvaz remains neutral with regard to jurisdictional claims in published maps and institutional affiliations.